International Journal of Solids and Structures 48 (2011) 163–174

Contents lists available at ScienceDirect

International Journal of Solids and Structures

journal homepage: www.elsevier.com/locate/ijsolstr

Determination of material intrinsic length and strain gradient hardening in microbending process

Li Hezong [a,b,*], Dong Xianghuai [a], Wang Qian [a], Shen Yu [a], A. Diehl [c], H. Hagenah [c], U. Engel [c], M. Merklein [c]

[a] National Die and Mold CAD Engineering Research Center, Shanghai Jiao Tong University, Shanghai, China
[b] Department of Mechanical and Electrical Engineering, Hebei University of Engineering, Handan, China
[c] Chair of Manufacturing Technology, University of Erlangen-Nuremberg, Erlangen, Germany

ARTICLE INFO

Article history:
Received 31 May 2010
Received in revised form 17 August 2010
Available online 25 September 2010

Keywords:
Gradient of effective plastic strain
Microbending
Springback
Material intrinsic length

ABSTRACT

Microbending experiments of pure aluminum show that the springback angles increase with the decrease of foil thickness, which indicates obvious size effects and attributes to plastic strain gradient hardening. Then a constitutive model, taking into accounts both plastic strain and plastic strain gradient hardening, is proposed to analyze the microbending process of thin foil. The model is based on the relationship between shear yield stress and dislocation density, in which the material intrinsic length is related to material properties and average grain numbers along the characteristic scale direction of part. It is adopted in analytical model to calculate the non-dimensional bending moment and predict the springback angle after microbending. It is confirmed that the predictions by the proposed hardening model agree well with the experimental data, while those predicted by the classical plasticity model cannot capture such size effects. The contribution of plastic strain gradient increases with the decrease of foil thickness and is independent on the bending angle.

1. Introduction

With the development of products toward miniaturization, the demands for metal micro parts are rapidly increasing in micro medical devices, electronics and telecommunication devices, micro system technology (MST) and micro electro-mechanical systems (MEMS), etc. (Geiger et al., 2001; Lee et al., 2008). In comparison with the micro machining and other micro technologies, the micro plastic forming is the most suitable and economic manufacturing process for mass production of micro metal components.

Recently, more and more experimental and theoretical researches on microbending of metal foils are implemented and obvious size effects are observed. Stölken and Evans have indicated that the non-dimensional bending moment increases when the foil thickness decreases from 50 μm to 12.5 μm in microbending tests of high purity nickel (Stölken and Evans, 1998). Suzuki has also observed the similar tendency in his microbending experiments of pure aluminum foils with thickness of 51 μm, 35 μm and 24 μm (Suzuki et al., 2009). In brass sheet bending process, Gau has found that springback angle is affected by the ratio of sheet thickness to mean grain size for thinner sheet, unlike the behavior of much thicker ones (Gau et al., 2007). Parasiz has investigated the effects of grain size and specimen size on the deformation distribution through the sheet thickness in microbending of CuZn30, and indicated that the plastic deformation will penetrate to the inner regions of sheet for the coarse grained structures when the specimen size is miniaturized (Parasiz et al., 2010). These experiments show that obvious size effects are observed and the springback angle is related to the mean grain size, but quantitative relations between them have not been established.

Although metal forming technology in macro scale is well established, it cannot be applied directly to metal microforming through scale down specimen and tooling size (Geiger et al., 2001). Therefore, it is necessary to develop a new plastic theory to explain the size effects in metal microforming. Fleck and Hutchinson have developed a phenomenological theory in micro scale, in which the hardening effects due to the strain gradient are considered (Fleck and Hutchinson, 2001). Based on this theory, Zhu has deduced a relationship between the non-dimensional bending curvature and the non-dimensional bending moment for metallic plates with a thickness from a few mm down to about 10 nm. At the micron scale, the strain gradient has a more dominant effect on the effective bending strength with thickness decreasing (Zhu and Karihaloo, 2008). Wang has analyzed the microbending behavior of metal foils, in which the strain gradient effects are significant on the bending stiffness when the beam thickness becomes comparable to the material intrinsic length (Wang et al., 2003). The size

* Corresponding author at: National Die and Mold CAD Engineering Research Center, Shanghai Jiao Tong University, Shanghai, China. Tel.: +86 021 62813435; fax: +86 021 62813435.
E-mail address: Lhzong@126.com (L. Hezong).

0020-7683/$ - see front matter © 2010 Elsevier Ltd. All rights reserved.
doi:10.1016/j.ijsolstr.2010.09.016

effects in microbending are discussed from dislocation dynamics and strain gradient plasticity by Zbib and Aifantis in Ref. (Zbib and Aifantis, 2003). In previous researches, the size effects on non-dimensional bending moment caused dominantly by plastic strain gradient have been analyzed in pure microbending process, however, the size effects on springback angles have not been investigated with detail.

Another hardening law are developed based on the Taylor's relation, in which the plastic work hardening is attributed to both statistically stored dislocations and geometrically necessary dislocations, and the latter is directly related to the plastic strain gradient (Gao et al., 1999; Huang et al., 2000; Nix and Gao, 1998). In the aforementioned gradient plasticity theories, the higher-order stress tensor work-conjugated to strain gradient is introduced in constitutive relations, and the additional unconventional boundary conditions related to the higher-order stresses are required, which leads to complexity in mathematical representations. This complexity can be avoided by using the gradient of the conventional effective plastic strain, instead of strain gradient tensor (Abu Al-Rub and Voyiadjis, 2005). This method is also adopted in present paper to deal with plastic strain gradient hardening. The prediction of non-dimensional bending moment and springback angle reveals the size effects in microbending process and agrees well with the experimental data.

The material intrinsic length is one of the important factors in plastic strain gradient theory and originally proposed for dimensional consistency, which is provided with various values by different investigators. Begley and Hutchinson (1998) have summarized the material length scale between 0.25 μm and 2 μm, and the fitting value of length scale is about 1.6 μm for an annealed metal (soft aluminum, copper and iron) and range from 0.5 μm to 1 μm for work hardened metal (hardened aluminum, copper and iron). It is showed that the harder the material is (work hardened or smaller grain size), the smaller the length scale is. This length is related to the free slip distance of dislocations, which decreases with hardness increasing or grain size decreasing. Nix and Gao (1998) have given the length scale 12 μm for annealed copper (single crystal) and 5.84 μm for cold worked copper (polycrystalline) based on the indentation experimental data (McElhaney et al., 1998). Nevertheless, Yuan and Chen (2001) have determined alternative value 20 μm and 6 μm respectively for the same experimental data. The intrinsic length is not consistent but it is obvious that the value of length scale for polycrystalline copper is only half of length for single crystal copper. Furthermore, Fleck et al. (1994) has found that the intrinsic length is in the range 2.6–5.1 μm and decreases with the wire diameter increasing and when the wire diameter increases up to 30 μm, it becomes larger again in microtorsion experiments with copper wires. Stölken and Evans (1998) have estimated the material length parameter as 5 μm based on their microbending tests of thin nickel foils. Haque and Saif (2003) has put forward a hypothesis that the intrinsic length is not a fixed parameter but depends on the grain sizes of material based on their nano-scale bending tests of aluminum. Voyiadjis and Abu Al-Rub (2005) have argued that the intrinsic length of materials is different due to the different value of macro-characteristic length and grain size of the specimen. If varied values of intrinsic length are taken in strain gradient hardening for microbending and microtorsion analyses, the predicted values can agree better with the experimental data. As mentioned above, all the researchers determine the intrinsic length by fitting the experimental data of microindentation, microbending or microtorsion tests, but no expression of intrinsic length scale is commonly accepted, and different authors estimate at different value even based on the same experimental data. Previous researches reveal that the material intrinsic length depends on many factors, including materials (e.g. copper, nickel, iron, and aluminum), material properties (e.g. shear modulus, initial yield strength, and hardness), material microstructure (e.g. Burger's vector, and grain size), and macro geometrical characteristic scale of specimens (e.g. foil thickness, wire diameter, or indentation depth).

In present paper, the springback behaviors after microbending of pure aluminum foils with five different thicknesses (0.5 mm, 0.2 mm, 0.1 mm, 0.05 mm, 0.025 mm) and same width (w = 10 mm) are investigated. In order to analyze the size effects presented in the experiments, a simplified constitutive model is proposed, which takes into account plastic strain gradient but does not introduce higher-order stress tensor. A semi-empirical expression is also proposed to determine the material intrinsic length, which is a function of shear modulus, initial yield strength, length of Burger's vector, grain size, and macro geometrical characteristic scale of the specimen. The constitutive model is adopted in analytical expressions to predict the non-dimensional bending moment and the springback angle after microbending. It is confirmed that the prediction results are in good agreement with the experimental data, while those obtained by using classical plasticity model cannot catch the size effects.

2. Microbending experiments

2.1. Material preparation

Pure aluminum (99.5%) is used in the microbending experiments. The Young's modulus is E = 69 GPa, the Poisson's ratio ν = 0.33, the shear modulus G = 26.3 GPa, and the length of Burger's vector $b = 2.86 \times 10^{-7}$ mm. In order to eliminate the effects of rolling texture, the aluminum foils are annealed at 550 °C for 1.5 h. There is many grains across the thickness for thicker foils, but there is only one or two grains for 0.025 mm thick foil, as shown in Fig. 1. ASTM E112-Heyn Lineal Intercept Procedure is used to determine the grain size of the specimens by analyzing the metallograph. The measure approach is to count on five or more blindly drawn lines along the longitudinal direction on the thickness section, then to calculate the average grain size. For all the cases, the number of grains intercepted by one or more straight lines sufficiently long to yield at least 50 intercepts. Hence, for the thinner foils, there exits a case that the average grain size is lager than the foil thickness, see Fig. 1a. Average grain size d and mean grain number n_G across thickness are given in Table 1.

Uniaxial tensile tests are performed, and the true stress-true strain curves are obtained, as shown in Fig. 2. At least five samples are repeated for each thickness, and the true stress–strain curve of each case is obtained by averaging the experimental data of these samples. The curves show a general trend that the yield strength decreases with the foil thickness decreasing, as the initial yield strengthen σ_{s0} shown in Table 1. The reason is that the share of surface grains on the overall volume is increasing with the foil thickness scaling down. These grains exhibit lower yield strength due to fewer constraints in contrast to grains positioned within the metal foil, leading to a decreasing material strength. However, the strength of the 0.5 mm thick foil is lower due to considerably lager grain size (see Table 1.) according to the Hall–Petch relation.

The following Swift's hardening model is used to fit the uniaxial tensile curves,

$$\sigma = K(\varepsilon_0 + \varepsilon)^n \tag{1}$$

where, σ is the flow stress and ε is the plastic tensile strain, respectively; $\sigma_{s0} = K\varepsilon_0^n$ is the initial yield strength of material (ε = 0); The parameters K, ε_0, n are obtained by curve fitting method, and given in Table 1.

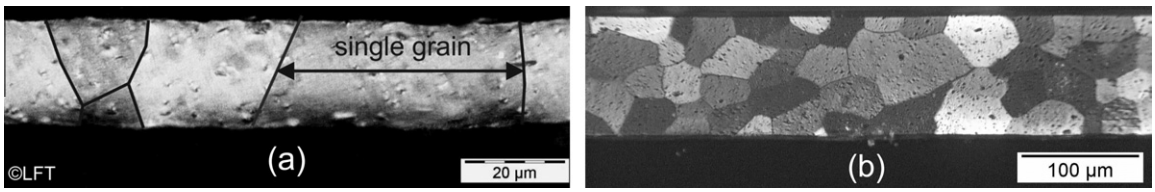

Fig. 1. Metallograph of aluminum foil with thickness (a) 0.025 mm and (b) 0.1 mm.

Table 1
Material and experimental set-up parameters.

h (mm)	λ	d (mm)	n_G	σ_{s0} (MPa)	K (MPa)	ε_0 (%)	n	l (mm)	l_n (mm)	$R_d = R_p$ (mm)	C (mm)	v (mm/min)
0.025	0.05	0.036	0.8	43.8	125.7	1.02	0.23	0.061	0.061	0.0625	0.03	0.5
0.05	0.1	0.036	1.6	44.6	172.1	0.95	0.29	0.060	0.038	0.125	0.06	1
0.1	0.2	0.052	2.0	47.0	154.2	1.23	0.27	0.053	0.027	0.25	0.12	2
0.2	0.4	0.038	5.4	48.1	152.7	0.66	0.23	0.051	0.09	0.5	0.24	4
0.5	1	0.075	6.5	34.4	100.8	0.35	0.19	0.098	0.012	1.25	0.6	10

l – the value of intrinsic length calculated by Eq. (9) without the mean grain numbers across thickness; l_n – the value of intrinsic length calculated by Eq. (10) with the mean grain numbers n_G across thickness.

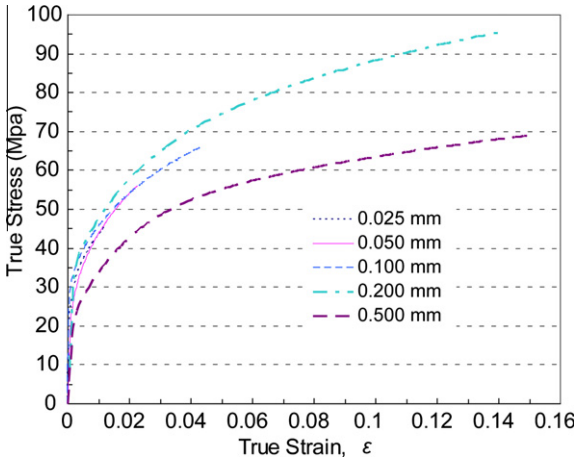

Fig. 2. Tensile true stress -true strain curves of pure aluminum foils.

2.2. Experimental procedure

In order to study on the size effects occurring in microbending processes, the springback behaviors of pure aluminum with different thicknesses are investigated. For this purpose, a scaled experiment set-up is established in LFT (illustrated in Fig. 3) (Diehl et al., 2008). In Fig. 3, $C = 1.2$ h denotes the clearance between die and punch, which is slightly larger than the sheet thickness h in order to prevent the sheet being squeezed.

In the experiments, all parameters, such as foil thickness h, die radius R_d, punch radius R_p, bending clearance C and punch velocity v, are changed proportionally according to the scaling factor λ ($\lambda = h/h_{\max}$, here $h_{\max} = 0.5$ mm). The values of the parameters are also given in Table 1.

A CCD camera is placed in front of the bending set-up to record the microbending process. As shown in Fig. 4, the bended angles, before and after bending springback, are measured from the recorded pictures by an edge detection algorithm, then the springback angle can be calculated. The bending angle $\theta_b = 30°, 45°, 65°$ is controlled by the punch stroke. Each experiment case is repeated five times and the springback angle is their average value. Error lines in Fig. 5 indicate the variation span of the experiment data of springback angle. In the experiments, the springback angle increases with foil thickness decreasing, which indicates obvious size effects, as shown in Fig. 5. It is the main purpose of this paper to develop a model to analyze this size effects.

3. Microbending theoretic analysis

According to classical bending theory, the main factors, which affect springback angle after bending, are the material properties

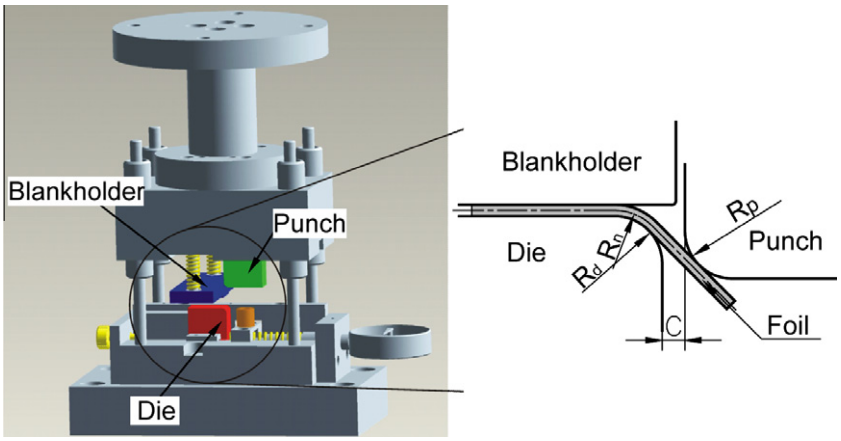

Fig. 3. Three-dimensional geometric model and schematic set-up of the free microbending tool.

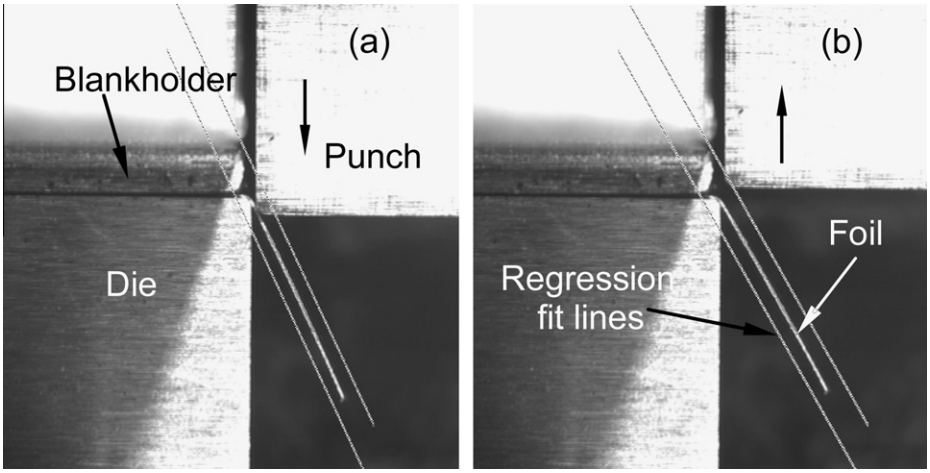

Fig. 4. CCD pictures to measure the angle of bended foil with regression fit line.

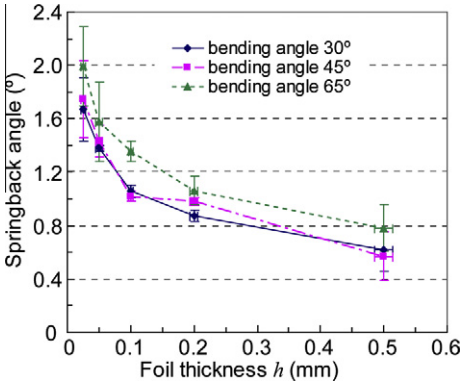

Fig. 5. Experimental data curve of springback angle versus foil thickness for Al.

(such as Young's modulus E and flow stress), the ratio of bending neutral radius (R_n) (see Fig. 3) to foil thickness R_n/h and bending clearance C etc. In the experiments, for all the foils, E, R_n/h and C are identical, hence the difference of springback angle can be attributed to flow stress. Since the hardening curves are no distinctly different in uniaxial tensile tests for all the foils (see Fig. 2), the hardening behavior related with plastic strain gradient should be the main factor affecting flow stress and leading to the size effects in microbending process. Therefore, a constitutive relation is proposed, in which the plastic strain gradient hardening is taken into account, and then it is applied to an analytical model of bending process to analyze the size effects of springback angle.

3.1. Constitutive relation

Illuminated by the relation between yield shear stress and dislocation density (Taylor, 1938), a hardening model has proposed in Refs. (Gao et al., 1999; Huang et al., 2000; Nix and Gao, 1998). Taylor's relation can be written as:

$$\begin{aligned}\tau &= \alpha G b\sqrt{\rho_T} = \alpha G b\sqrt{\rho_S + \rho_G}\\ \sigma &= M\tau\end{aligned} \tag{2}$$

where, α is an empirical material constant ranging between 0.1 and 0.5; ρ_T, ρ_S and ρ_G are, respectively, the total dislocation density, the statistically stored dislocation density and the geometrically necessary dislocation density; M is Taylor coefficient, which reflects the ratio of tensile yield strength σ to shear yield strength τ. In classical plasticity, only plastic strain, related with the statistically stored dislocation density ρ_S, is considered, however the geometrically necessary dislocation density ρ_G may become important in some microforming processes.

A relation between the plastic strain gradient and the geometrically necessary dislocation density is assumed as,

$$\nabla\varepsilon = \rho_G b \tag{3}$$

where $\nabla\varepsilon$ denotes strain gradient.

For bending deformation, Eq. (3) can be deduced based on a simplified model as shown in Fig. 6a. If there is a positive edge dislocation in lattice, the length of top edge will be longer than the bottom one by a distance b (length of the Burger's vector), since an extra half plane of atoms is inserted. In bending process, there exists the length difference between the top and the bottom edges, thus, it is necessary that a series of edge dislocations (so-called the geometrically necessary dislocation) should be piled in the crystal lattice after plastic bending.

For the plastic bending deformation of single crystal as shown in Fig. 6a, the difference between the top and the bottom edges is: $(R_i + h)\theta - R_i\theta = h\theta$, where R_i is the inner radius of the bending foil and θ is the bending angle. Therefore, the number of piled edge dislocations is $h\theta/b$ in the whole crystal. The section area of the bending crystal is $R_n\theta h$, so the geometrically necessary dislocation density is:

$$\rho_G = \frac{h\theta/b}{R_n\theta h} = \frac{1}{R_n b} \tag{4}$$

On the other hand, the gradient (along the thickness direction) of plastic strain along longitudinal direction of the sheet is:

$$\nabla\varepsilon = \frac{\frac{(R_i+h)\theta - R_n\theta}{R_n\theta} - \frac{R_i\theta - R_n\theta}{R_n\theta}}{h} = \frac{1}{R_n} = \kappa_n \tag{5}$$

where, κ_n is the curvature of the neutral layer and $R_n = R_i + h/2$ is the neutral radius.

Eq. (3) can be deduced from Eqs. (4) and (5).

Eqs. (4) and (5) show that if the foil thickness and the tooling size scale down, the smaller is the neutral radius R_n, the larger is the geometrically necessary dislocation density ρ_G and the strain gradient $\nabla\varepsilon$. Therefore, the flow stress will increase according to the Eq. (2), and then the springback angle of bending will increase, too.

The mechanism of plastic strain gradient hardening with polycrystal across foil thickness is different from single crystal in bending process. Simplified bending models are shown in Fig. 6, where Fig. 6a illustrates the case of a single crystal, and Fig. 6b illustrates

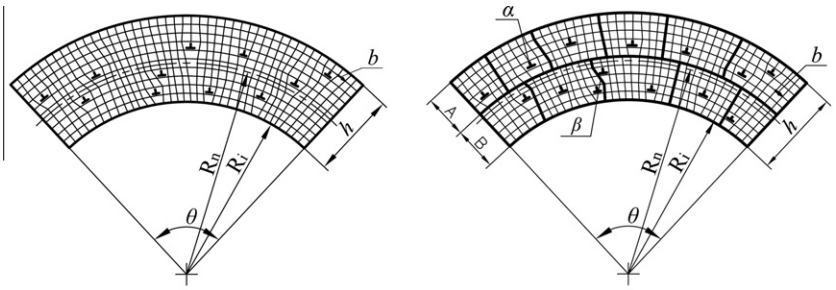

(a) single crystal along thickness direction (b) two crystals along thickness direction

Fig. 6. Geometrically necessary dislocation morphology in plastic bending of metal.

the case with two layers grains across the foil thickness. It is assumed that in both cases, the bending conditions are identical, so their average geometrically necessary dislocation densities are equal, and the mean strain gradient is equal to each other according to the Eqs. (4) and (5). However, the distribution and the effects of geometrically necessary dislocations on material hardening are different apparently. For the polycrystalline foil, the influence of stress field of geometrically necessary dislocations in outer layer grains on the inner layer grains will be reduced because of the grain boundary. For example, an edge dislocation in outer layer grains, such as the edge dislocation α in Fig. 6b, will distort the lattice around the dislocation in this grain, but will not, or only slightly, distort the neighboring grain to inner layer grains. In addition, the geometrically necessary dislocations may be arranged to form the grain boundary as β in Fig. 6b, which will hinder the movement of other dislocations and increase the material strength. This hardening mechanism is due to the statistically stored dislocations and is explained by the classical plasticity model without considering the plastic strain gradient. The above-mentioned mechanisms weaken the hardening effects of the geometrically necessary dislocations for polycrystal. However, Eq. (5) cannot take into account such weakening phenomenon when grain numbers across the characteristic scale of specimens increases. The weakening effects are grown up for the case of multilayer grain across thickness, and the more is the grain number across the foil thickness, the weaker is the effect to the material work hardening. Furthermore, based on Taylor relation, for polycrystalline specimens, because the grain boundary prevents the movement of dislocations, the strain hardening owing to the statistically stored dislocations will be increased. Then if the total dislocation density is assumed to equal to each other in both Fig. 6a and b, the share of hardening effects by geometrically necessary dislocations will decrease in case of multilayer grains compared with the single crystal. For metal plastic forming, Li and Chou (1970) have expressed the relation of strain, dislocation density and grain sizes as follows:

$$\rho_S = \frac{\varepsilon}{kbd} \tag{6}$$

where, k is a constant parameter, d is the average grain size, b is the length of the Burger's vector, and ε is the plastic strain. If the foil thickness and the die radius are constant in microbending, (that is, the plastic strain ε is invariable), the work hardening due to statistically stored dislocations for fine grain material is more than that for coarse grain material. The reason is that there are more grain boundaries to prevent the slip of dislocations for fine grain material and cause the statistically stored dislocations to pile up. As a result, the hardening effect by geometrically necessary dislocations is relative weaker. In other words, if the foil thickness is very thin, at the same time, the grain size is very small, the strain gradient hardening become weaker and weaker, even neglectable, which is similar to macro forming that there are many grains across the thickness and without strain gradient hardening exits.

Therefore, with increasing of the grain numbers across the geometrical characteristic scale direction of the specimen, the strain hardening due to statistically stored dislocations will increase, and the strain gradient hardening due to geometrically necessary dislocations will decrease. For the microbending process, the geometrical characteristic scale of the specimen is foil thickness. In this paper, the increase of strain hardening with the grain numbers through the thickness is considered into the uniaxial tensile hardening model. While the decrease of strain gradient hardening caused by the decrease of lattice distortion extent from the geometrically necessary dislocations due to grain boundary will be considered into the modified intrinsic length, which is discussed in details in the following section. The modified intrinsic length is introduced to calculate the non-dimensional bending moment and the springback angle in microbending process, and the prediction results fit the experimental data better.

It is assumed that the stress–strain relation is expressed as the following equation:

$$\sigma = Kf(\varepsilon) \tag{7}$$

For Swift's hardening model, $f(\varepsilon) = (\varepsilon_0 + \varepsilon)^n$, which is a function of conventional plastic strain. Using similar method as in Refs. (Gao et al., 1999; Huang et al., 2000; Xue et al., 2002) and taking the plastic strain gradient hardening into account in Eq. (7), a flow stress model is proposed as:

$$\sigma = K[f^{\beta}(\varepsilon) + (l|\nabla\varepsilon|)^{\beta}]^{\frac{1}{\beta}} \tag{8}$$

where, $f(\varepsilon)$ and $l|\nabla\varepsilon|$, represents the contribution of the plastic strain and the plastic strain gradient, that is statistically stored dislocations and geometrically necessary dislocations, respectively, to the flow stress; β is an adjusting parameter; l is the material intrinsic length.

Xue has proposed the following equation to calculate the intrinsic length (Xue et al., 2002),

$$l = 18\alpha^2\left(\frac{G}{\sigma_{s0}}\right)^2 b \tag{9}$$

On the other hand, the material intrinsic length is usually determined by fitting the experimental data of microbending, microtorsion or microindentation, in which the plastic strain gradient hardening appears. The intrinsic lengths of the foils determined by Eq. (9) are given in Table 1, denoted by l.

Based on the strain gradient theory and the intrinsic length Eq. (9), Zhu and Karihaloo (2008) and Wang et al. (2003) have investigated the relation of non-dimensional bending curvature and the non-dimensional bending moment. They have indicated that for the sheets with the same thickness, the non-dimensional bending

moment increases with increasing non-dimensional bending curvature, i.e. with increasing surface strain and the strain gradient.

Considering the above-mentioned weakening effects of the boundary between multilayer grains across thickness on the geometrically necessary dislocations, Eq. (9) is adjusted as:

$$l = 18\alpha^2\left(\frac{G}{\sigma_{s0}}\right)^2\frac{b}{n_G} \tag{10}$$

where, n_G is the numbers of grain layer across the foil thickness, which are also given in Table 1. In case of single grain layer foils ($n_G = 1$), Eq. (10) is the same as Eq. (9). When there are multilayer grains across the foil thickness ($n_G > 1$), the material intrinsic length l will decrease by $1/n_G$ according to Eq. (10), that is, the relative contribution of strain gradient hardening caused by geometrically necessary dislocations will decrease by $1/n_G$. It is found that the predicted non-dimensional bending moment and springback angles by using Eq. (10) are much closer to the experimental data than those by using Eq. (9). If the average grain number is less than 1.0, the material intrinsic length is calculated by Eq. (10) setting $n_G = 1$ because there are no grain boundaries through the thickness. The material intrinsic lengths of the foils determined by Eq. (10) are also given in Table 1, denoted by l_n and when using Eq. (10), the minimal $n_G \geqslant 1$ is assumed.

Based on Swift's hardening model (Eq. (1)) and Eq. (8), a modified hardening law with strain gradient hardening is proposed by the authors as:

$$\sigma = K[(\varepsilon_0 + \bar{\varepsilon})^{\beta n} + (l|\nabla\varepsilon|)^{\beta}]^{\frac{1}{\beta}} \tag{11}$$

where, $\bar{\varepsilon} = \left[(2/3)\varepsilon'_{ij}\varepsilon'_{ij}\right]^{1/2}$ is the conventional effective plastic strain. In this paper, $\alpha = 0.18$ and $\beta = 1$ are determined by fitting experimental results to capture the size effects.

Fleck has proposed a definition of effective plastic strain with the contribution of strain gradient, $\bar{\varepsilon}_T$, for microbending as (Fleck and Hutchinson, 1997):

$$\bar{\varepsilon}_T = \left\{\bar{\varepsilon}^{\mu} + \left[l_S^2\eta'^{(1)}_{ijk}\eta'^{(1)}_{ijk}\right]^{\mu/2} + \left[(2/3)l_R^2\chi_{ij}\chi_{ij}\right]^{\mu/2}\right\}^{1/\mu} \tag{12}$$

where, l_S is the internal material length for stretch gradient; l_R is that for rotation gradient; Let η_{ijk} denote the second gradient of displacement u_i, i.e. $\eta_{ijk} = u_{k,ij}$, then $\eta^{(1)}_{ijk} = \eta^S_{ijk} - \xi_{ijk}$ is the first deviatoric invariant of the second gradient of displacement, where $\eta^S_{ijk} = \frac{1}{3}\left(\eta'_{ijk} + \eta'_{jki} + \eta'_{kij}\right)$, $\eta'_{ijk} = \frac{1}{4}(\delta_{ik}\eta_{jpp} + \delta_{jk}\eta_{ipp})$, $\xi_{ijk} = \frac{1}{5}\left(\delta_{ij}\eta^S_{kpp} + \delta_{jk}\eta^S_{ipp} + \delta_{ki}\eta^S_{jpp}\right)$; $\chi_{ij} = -e_{ist}\varepsilon_{js,t} = e_{its}\varepsilon_{js,t}$ is the deformation curvature. δ_{ij} is the Kronecker delta and e_{ijk} is the permutation tensor. Original studies of Fleck and Hutchinson and others favor $\mu = 2$ primarily on mathematical grounds (Evans and Hutchinson, 2009), but the non-dimensional bending moment results for $\mu = 1$ give a slightly better fit to the experimental data (Evans and Hutchinson, 2009; Stölken and Evans, 1998), and so $\mu = 1$ is adopted here.

Let $\bar{\varepsilon}_G$ denote the item related with plastic strain gradient in Eqs. (11) and (12):

$$\bar{\varepsilon}_G = l|\nabla\varepsilon| = \left\{\left[l_S^2\eta'^{(1)}_{ijk}\eta'^{(1)}_{ijk}\right]^{\frac{\mu}{2}} + \left[(2/3)l_R^2\chi_{ij}\chi_{ij}\right]^{\frac{\mu}{2}}\right\}^{\frac{1}{\mu}} \tag{13}$$

then, the effective strain gradient $|\nabla\varepsilon|$ is:

$$|\nabla\varepsilon| = \left\{\left[\left(\frac{l_S}{l}\right)^2\eta'^{(1)}_{ijk}\eta'^{(1)}_{ijk}\right]^{\frac{\mu}{2}} + \left[\frac{2}{3}\left(\frac{l_R}{l}\right)^2\chi_{ij}\chi_{ij}\right]^{\frac{\mu}{2}}\right\}^{\frac{1}{\mu}} \tag{14}$$

where, $l = \left(\frac{2}{\sqrt{5}}l_s + \frac{1}{\sqrt{2}}l_R\right)$.

It is very complicated to calculate strain gradients $|\nabla\ \varepsilon|$ by Eq. (14), which is required in the calculation of $\bar{\varepsilon}_G$ by Eq. (13). Hence, a simplified method to calculate $\bar{\varepsilon}_G$ is adopted as follows, in which the gradient of conventional effective plastic strain is involved instead of the tensor operation in Eq. (14).

$$\bar{\varepsilon}_G = l|\nabla\bar{\varepsilon}| \tag{15}$$

where, $|\nabla\bar{\varepsilon}|$ is the effective value, or the modulus, of the gradient of the conventional effective plastic strain.

Then the constitutive relation is rewritten from Eq. (11) as:

$$\bar{\sigma} = K\left[(\varepsilon_0 + \bar{\varepsilon})^n + l|\nabla\bar{\varepsilon}|\right] \tag{16}$$

3.2. Gradient of effective plastic strain

The local coordinate system is established as shown in Fig. 7, in which ξ_1, ξ_2, ξ_3 are along the length, thickness and width directions, respectively. Since the foil width w is much larger than the thickness h, plane strain is assumed.

The true strain along the longitudinal directions ξ_1 for any layer ξ_2 is:

$$\varepsilon_1 = \ln(1 + \kappa_n\xi_2) \tag{17}$$

The engineering strain is:

$$e_1 = \kappa_n\xi_2 \tag{18}$$

The maximum engineering strain $e_{\max}$, on the foil surface of the bending deformation area, depends on the foil thickness and the bending radius of the neutral layer and is defined as:

$$e_{\max} = \frac{h/2}{R_n} \tag{19}$$

Because of the smaller bending clearance relative to the foil thickness ($C - h = 0.2$ h) in bending experiments, the foil inner surface is assumed to contact with the die and the bending radius is equal to the die radius. Thus, the bending radius of the neutral layer can be calculated:

$$R_n = R_d + h/2 \tag{20}$$

Because the strain is relatively small in our bending experiments ($e_{\max} = 0.167$), for simplicity, it is assumed:

$$\varepsilon_1 = e_1 = \kappa_n\xi_2 \tag{21}$$

The gradient along foil thickness of the strain (along the length direction) is:

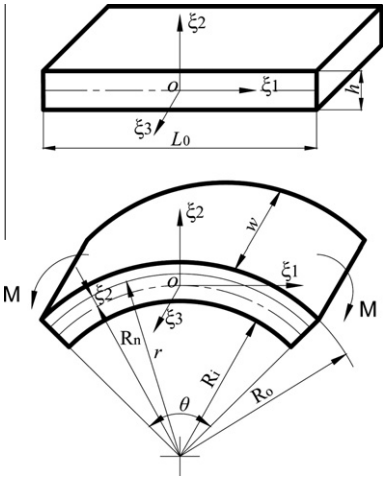

Fig. 7. Coordinate diagram defining the spatial quantities for the pure moment bending.

$$\nabla\varepsilon = \frac{2\varepsilon_{\max}}{h} \tag{22}$$

From Eqs. (19), (20) and (22), this strain gradient can also be deduced:

$$\nabla\varepsilon = \frac{1}{R_n} = \kappa_n \tag{23}$$

Eq. (23) is the same as Eq. (5), which is derived from the hypothesis of the geometrically necessary dislocation morphology in plastic bending region of metal, and therefore the hypothesis is reasonable for bending.

Since the foil thickness and the die radius are scaled by λ, the foil surface strain remains constant ($\varepsilon_{\max} = e_{\max} = 0.167$) for all thickness foils in our microbending experiments, but the strain gradient increases with the foil thickness decreasing. That is to say, the hardening due to the statistically stored dislocations is similar for all foil thickness according to the uniaxial tensile tests and the size effects of springback angle are mainly attributable to the geometrically necessary dislocations in microbending process.

For plane strain state, $\varepsilon_3 = 0$, the thickness strain is obtained by volume constancy condition: $\varepsilon_2 = -\varepsilon_1$. The conventional effective plastic strain is:

$$\bar{\varepsilon} = \sqrt{\frac{2}{3}\varepsilon'_{ij}\varepsilon'_{ij}} = \frac{2}{\sqrt{3}}\kappa_n\xi_2 \tag{24}$$

then, the gradient of effective plastic strain is:

$$\nabla\bar{\varepsilon} = \begin{bmatrix} 0 & \frac{2}{\sqrt{3}}\kappa_n & 0 \end{bmatrix} \tag{25}$$

$$|\nabla\bar{\varepsilon}| = \frac{2}{\sqrt{3}}\kappa_n \tag{26}$$

$$\bar{\varepsilon}_G = l|\nabla\bar{\varepsilon}| = \frac{2}{\sqrt{3}}l\kappa_n \tag{27}$$

3.3. Strain gradient and stress based on the displacement assumption

3.3.1. Displacement, strain and strain gradient

Based on the microbending experimental set-up (Shown in Fig. 3), the detailed geometric model of microbending deformation is illustrated in Fig. 8.

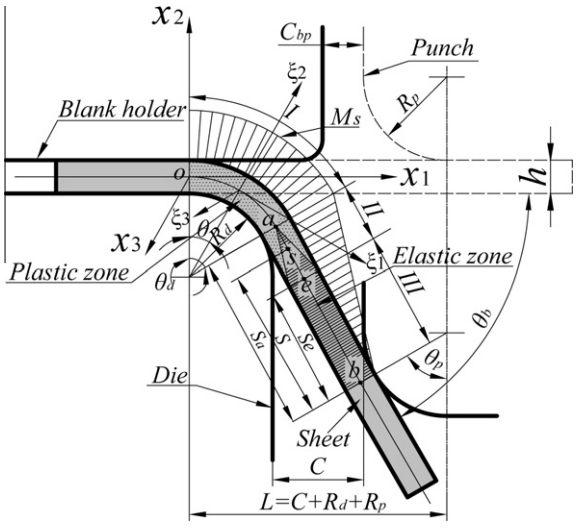

Fig. 8. Schematic diagram of the microbending.

For the microbending, the displacement field in the local coordinate system (Shown in Fig. 8) is assumed as (Stölken and Evans, 1998):

$$u_1 = \kappa_n\xi_1\xi_2, \quad u_2 = -\kappa_n\left(\xi_1^2 + \xi_2^2\right)/2, \quad u_3 = 0 \tag{28}$$

from it, the strain tensor is obtained,

$$[\varepsilon_{ij}] = \begin{bmatrix} \kappa_n\xi_2 & 0 & 0 \\ 0 & -\kappa_n\xi_2 & 0 \\ 0 & 0 & 0 \end{bmatrix} \tag{29}$$

The conventional effective strain is:

$$\bar{\varepsilon} = \sqrt{\frac{2}{3}\varepsilon'_{ij}\varepsilon'_{ij}} = \frac{2}{\sqrt{3}}\kappa_n\xi_2 \tag{30}$$

The stretch strain gradient η_{ijk} is:

$$[\eta_{ijk}] = \left[\begin{pmatrix} 0 & \kappa_n & 0 \\ -\kappa_n & 0 & 0 \\ 0 & 0 & 0 \end{pmatrix} \begin{pmatrix} \kappa_n & 0 & 0 \\ 0 & -\kappa_n & 0 \\ 0 & 0 & 0 \end{pmatrix} \begin{pmatrix} 0 & 0 & 0 \\ 0 & 0 & 0 \\ 0 & 0 & 0 \end{pmatrix} \right] \tag{31}$$

and the rotational strain gradient is:

$$[\chi_{ij}] = \begin{bmatrix} 0 & 0 & \kappa_n \\ 0 & 0 & 0 \\ 0 & 0 & 0 \end{bmatrix} \tag{32}$$

The first deviatoric invariant of the strain gradient is:

$$\left[\eta'^{(1)}_{ijk}\right] = \left[\begin{pmatrix} 0 & \frac{7}{15}\kappa_n & 0 \\ \frac{7}{15}\kappa_n & 0 & 0 \\ 0 & 0 & 0 \end{pmatrix} \begin{pmatrix} \frac{7}{15}\kappa_n & 0 & 0 \\ 0 & -\frac{9}{15}\kappa_n & 0 \\ 0 & 0 & 0 \end{pmatrix} \begin{pmatrix} 0 & 0 & 0 \\ 0 & 0 & \frac{2}{15}\kappa_n \\ 0 & \frac{2}{15}\kappa_n & 0 \end{pmatrix} \right] \tag{33}$$

The effective strain gradient is obtained by Eq. (14) ($\mu = 1$):

$$|\nabla\varepsilon| = \left[\left(\frac{l_S}{l}\right)^2 \eta'^{(1)}_{ijk}\eta'^{(1)}_{ijk}\right]^{\frac{1}{2}} + \left[\frac{2}{3}\left(\frac{l_R}{l}\right)^2 \chi_{ij}\chi_{ij}\right]^{\frac{1}{2}} = \frac{2}{\sqrt{3}}\kappa_n \tag{34}$$

Then the item related with strain gradient in Eq. (13) is:

$$\bar{\varepsilon}_G = l|\nabla\varepsilon| = \frac{2}{\sqrt{3}}l\kappa_n \tag{35}$$

Eqs. (34) and (35), which is deduced from the assumption of displacement field, is completely consistent with Eqs. (26) and (27) respectively, which is from the gradient of conventional effective strain. Therefore, the gradient of conventional effective strain can be used to analyze the size effects in microbending without tensor operation.

The total effective strain considering the plastic strain gradient is calculated by Eq. (12) ($\mu = 1$):

$$\bar{\varepsilon}_T = \bar{\varepsilon} + \bar{\varepsilon}_G = \frac{2}{\sqrt{3}}(\varepsilon_1 + l\kappa_n) \tag{36}$$

Eqs. (24) or (30) and (27) or (35) are substituted into Eq. (16) or (11), and the constitutive relation used in the analytical model is obtained ($\beta = 1$):

$$\bar{\sigma} = K\left[\left(\varepsilon_0 + \frac{2}{\sqrt{3}}\kappa_n\xi_2\right)^n + \frac{2}{\sqrt{3}}l\kappa_n\right] \tag{37}$$

3.3.2. Stress

For foil microbending, the radial stress normal to the foil is assumed to be zero (plane stress state), and only stresses along the longitudinal and width direction are considered, i.e. $\sigma_2 = 0$, $\sigma_3 = \frac{1}{2}\sigma_1$.

Thus, the effective stress is:

$$\bar{\sigma} = \sqrt{\frac{3}{2}\sigma'_{ij}\sigma'_{ij}} = \frac{\sqrt{3}}{2}\sigma_1 \tag{38}$$

In bending deformation, a foil section may be deformed elastically, or contains the elastic core, as shown in Fig. 9. In such elastically deformed region, the stress is:

$$\sigma_1 = \frac{E}{1-\nu^2}\varepsilon_1 = E'\varepsilon_1 \quad 0 \leqslant \bar{\varepsilon}_T \leqslant \varepsilon_e \tag{39}$$

where ε_e is the elastic strain limit and $E' = \frac{E}{1-\nu^2}$.

In the plastically deformed region, the constitutive equation is obtained by substituting Eq. (38) into Eq. (37):

$$\sigma_1 = \frac{2}{\sqrt{3}}K\left[\left(\varepsilon_0 + \frac{2}{\sqrt{3}}\kappa_n\xi_2\right)^n + \frac{2}{\sqrt{3}}l\kappa_n\right] \quad \bar{\varepsilon}_T \geqslant \varepsilon_e \tag{40}$$

3.4. Bending moment

3.4.1. Elastic bending moment

The bending moment is calculated as:

$$M = \int_0^h \sigma_1\xi_2 w d\xi_2 = M_e + M_p \tag{41}$$

where, M_e is the elastic bending moment caused by the stress within the elastic core and M_p is that within the plastically deformed region, as shown in Fig. 9.

From Eqs. (41) and (39), the elastic bending moment can be calculated as:

$$M_e = \int_{-\xi_{2e}}^{\xi_{2e}} \sigma_1\xi_2 w d\xi_2 = \frac{2w}{3}E'\kappa_n\xi_{2e}^3 \tag{42}$$

For pure elastic bending ($\xi_{2e} = \frac{h}{2}$), the elastic bending moment is:

$$M_E = \frac{w}{12}E'\kappa_n h^3 \tag{43}$$

3.4.2. Plastic bending moment

The plastic component of bending moment is obtained with Eqs. (41) and (40):

$$\begin{aligned} M_p &= 2\int_{\xi_{2e}}^{h/2} \sigma_1\xi_2 w d\xi_2 = \frac{4Kw}{\sqrt{3}}\int_{\xi_{2e}}^{h/2}\left[\left(\varepsilon_0 + \frac{2}{\sqrt{3}}\kappa_n\xi_2\right)^n + \frac{2}{\sqrt{3}}\kappa_n l\right]\xi_2 d\xi_2 \\ &= \frac{4Kw}{\sqrt{3}}\left\{\frac{l\kappa_n}{\sqrt{3}}\left(\frac{h^2}{4} - \xi_{2e}^2\right) + \frac{3}{4\kappa_n^2}\left[\frac{1}{n+2}\left(\left(\varepsilon_0 + \frac{h\kappa_n}{\sqrt{3}}\right)^{n+2}\right.\right.\right. \\ &\quad \left.\left.\left. - \left(\varepsilon_0 + \frac{2\kappa_n\xi_{2e}}{\sqrt{3}}\right)^{n+2}\right) - \frac{\varepsilon_0}{n+1}\left(\left(\varepsilon_0 + \frac{h\kappa_n}{\sqrt{3}}\right)^{n+1} - \left(\varepsilon_0 + \frac{2\kappa_n\xi_{2e}}{\sqrt{3}}\right)^{n+1}\right)\right]\right\} \end{aligned} \tag{44}$$

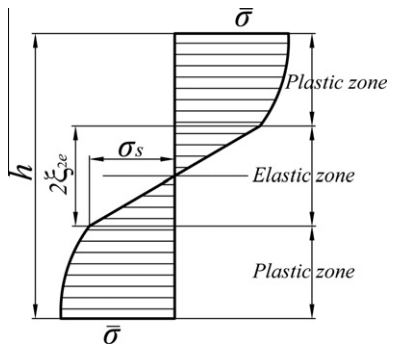

Fig. 9. Stress distribution along foil thickness direction.

For fully plastic bending ($\xi_{2e} = 0$), the plastic bending moment is given by:

$$\begin{aligned} M_P = \frac{Kw}{\sqrt{3}}\left\{\frac{l\kappa_n h^2}{\sqrt{3}} + \frac{3}{\kappa_n^2}\left[\frac{1}{n+2}\left(\left(\varepsilon_0 + \frac{h\kappa_n}{\sqrt{3}}\right)^{n+2} - (\varepsilon_0)^{n+2}\right)\right.\right. \\ \left.\left. - \frac{\varepsilon_0}{n+1}\left(\left(\varepsilon_0 + \frac{h\kappa_n}{\sqrt{3}}\right)^{n+1} - (\varepsilon_0)^{n+1}\right)\right]\right\} \end{aligned} \tag{45}$$

3.4.3. Bending moment distribution along longitudinal direction

A curvilinear coordinate is defined starting from point b toward point o, as shown in Fig. 8. After bending, the center line of the foil is assumed to consist of two segments: one is a straight line from point b to a, the other is an arc from point a to o, where point a is the tangential point. For simplicity, an approximated bending moment distribution is assumed as follows: zone from point b to e (zone *III*) is in pure elastic bending; zone from point e to a (zone *II*) is in elastic–plastic deformation; and die-sheet contact zone from point a to o (zone *I*) is in pure plastic deformation. It is assumed that the bending moment varies linearly from point b to a.

Therefore, the bending moment along longitudinal direction can be calculated as follows:

$$\begin{aligned} M_S &= M_P, \quad \text{if } S \geqslant S_a \\ M_S &= \frac{S}{S_a}M_P, \quad \text{if } S < S_a \end{aligned} \tag{46}$$

where, S is the curve length from point b to some point s.

The microbending deformation zone and the bending moment distribution are illustrated in the Fig. 8.

3.5. Springback angle after bending

After springback, if the neutral radius of the bended foil changes from R_n to R'_n, the curvature change before and after bending springback is:

$$\Delta\kappa_s = \frac{1}{R_n} - \frac{1}{R'_n} = \frac{M_S}{E'I} \tag{47}$$

where, M_S is the bending moment at a section of the sheet; $I = \frac{wh^3}{12}$ is the second moment of area.

The springback angle of an infinitesimal segment of the bended foil is obtained as:

$$d\theta_s = \Delta\kappa_s dS = \frac{M_S}{E'I}\cdot dS \tag{48}$$

where, dS is the segment length. The total springback angle of the bended foil can be calculated by integrating Eq. (48) across the total bending span:

$$\theta_s = \int_0^{S_a}\frac{M_P}{E'I}\frac{S}{S_a}dS + \int_{S_a}^{S_o}\frac{M_P}{E'I}dS = \frac{M_P}{E'I}\left(\frac{1}{2}S_a + \widehat{S}_{oa}\right) \tag{49}$$

where, $\widehat{S}_{oa}$ is the die-sheet contact arc length.

$$\widehat{S}_{oa} = \left(R_d + \frac{h}{2}\right)\cdot\theta_d \tag{50}$$

Reference to the geometric relation in the Fig. 8, the length S_a from point b to a can be calculated as:

$$S_a = \left[L - \left(R_d + \frac{h}{2}\right)\sin\theta_d - \left(R_p + \frac{h}{2}\right)\sin\theta_p\right]/\cos\theta_b \tag{51}$$

where, θ_b is the bending angle, which is assumed as the same value as the die-sheet contact angle θ_d and the punch-sheet contact angle θ_p; $L = C + R_d + R_p$, see Fig. 8.

Eq. (49) is rewritten to calculate the normalized bending moment M/wh^2 with measured springback angles, θ_s:

$$\frac{M}{wh^2} = \frac{E'h}{12} \cdot \frac{\theta_s}{\widehat{S}_{oa} + \frac{1}{2}S_a} \tag{52}$$

If the bending clearance is equal to the foil thickness ($C = h$), and the die-sheet contact angle $\theta_d = \pi/2$, by Eq. (51), $S_a = 0$ is obtained, and then the normalized bending moment is:

$$\frac{M}{wh^2} = \frac{E\prime h}{12} \cdot \frac{\theta_s}{\widehat{S}_{oa}} = \frac{E'h}{12}\left(\frac{1}{R_n} - \frac{1}{R'_n}\right) \tag{53}$$

In Ref. (Stölken and Evans, 1998), a expression similar to Eq. (53) is used to determine the normalized bending moment by measured θ_s. Moreover, in order to study on the plasticity size effects more clearly, it is necessary to remove the effect of initial tensile yield strength σ_{s0} from the bending moment, and so, the non-dimensional bending moment $\frac{M}{\sigma_{s0}wh^2}$ is used in the following analysis.

4. Results and discussions

4.1. Non-dimensional bending moment prediction and material intrinsic length

Fig. 10a and b show curves of non-dimensional bending moment and non-dimensional bending curvature $\kappa_n h$ in microbending process. The hollow dots illustrate the experimental data, in which each dot from top to down is corresponding to the thickness from 0.025 mm up to 0.5 mm, respectively. The curves marked $l = 0$ are corresponding to classical plasticity for different thickness foils, in which the non-dimensional bending moments are the same and the curves are superposed one another. Therefore, the classical plasticity theory cannot express the size effects of hardening in microbending process. In Fig. 10a, the non-dimensional bending moment is calculated, in which the material intrinsic length by Eq. (9) is not variable with average grain numbers along the foil thickness, and in Fig. 10b, in which the material intrinsic length by Eq. (10) is variable with the average grain numbers along the foil thickness.

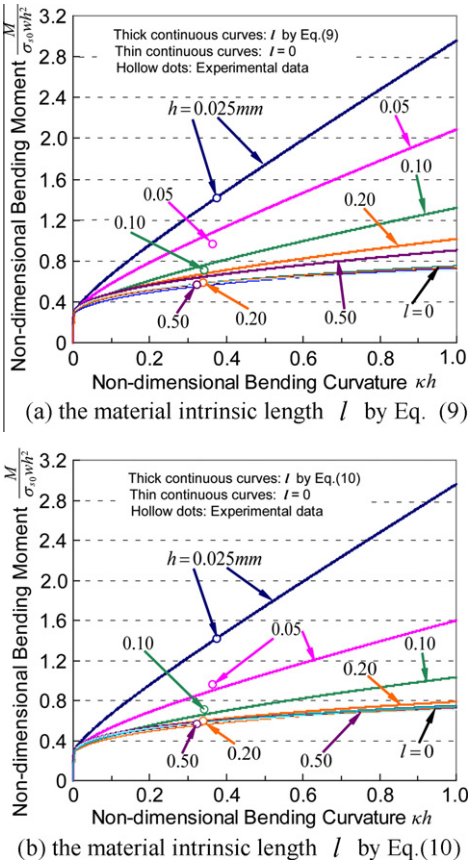

Fig. 10. The non-dimensional bending moment versus the non-dimensional curvature for different foil thickness h.

The results in Fig. 10a are similar to those obtained by Wang et al. (2003), in which the non-dimensional bending moment increases with the non-dimensional bending curvature increasing, but there is no dropping as those found by Zhu and Karihaloo (2008). Fig. 10a also shows that the difference of the non-dimensional bending moments between calculated from plastic strain gradient and material intrinsic length Eq. (9) and calculated from the classical plasticity, which is the strain gradient hardening effect, is decreasing with the foil thickness increasing. Nevertheless, even though the sheet thickness is up to macro scale, e.g. 0.5 mm, the non-dimensional bending moment is much more than that from classical plasticity theory. In addition, the prediction of non-dimensional bending moment based on the strain gradient and the material intrinsic length Eq. (9) is much larger than the experimental data except for the case of the thickness 0.025 mm, but for the thicker foils, 0.2 mm and 0.5 mm, the results based on classical plasticity theory are approaching to the experimental data. Fig. 10b based on the material intrinsic length Eq. (10) also shows that there exist the size effects of strain gradient hardening for the thinner foils and the prediction results are much closer to the experimental data than Fig. 10a. For the thicker foil, 0.5 mm, the prediction of non-dimensional bending moment is approaching to the classical plasticity results and there are hardly any size effects of strain gradient hardening. In fact, the strain gradient hardening effects are insignificant for foil thickness larger than 0.2 mm, which agrees with the experimental data by Gau et al. (2007). In their experiments, when the sheet thickness is larger than 0.35 mm for brass, the springback angle amount is consistent with the macro scale sheet in bending process.

Fig. 11a and b show curves of non-dimensional bending moment versus foil thickness h. The thick continuous curves are plotted from the strain gradient theory, and the thin continuous curves are plotted from the classical plasticity theory ($l = 0$). In Fig. 11a, the material intrinsic length is calculated from Eq. (9), and in Fig. 11b, it is calculated from Eq. (10). Fig. 11a and b show that the non-dimensional bending moment based on the classical plasticity theory increases with the foil thickness increasing for the same die radius bending, and with the die radius decreasing for the same foil thickness, which is because of the increase of the maximum strain or the surface strain according to Eq. (19). The thick continuous curves show that the non-dimensional bending moment based on the strain gradient theory is larger than the results based on the classical plasticity theory for the same die radius. However, the difference between them decreases with the foil thickness increasing, which is because the strain gradient becomes smaller according to Eqs. (20) and (23), on the contrary, the strain gradient hardening is significant for thinner foils.

Furthermore, Fig. 11a also shows that for the macro scale thickness sheet (e.g. thickness up to 1.0 mm), whether the die radius is smaller (e.g. $R_d = 0.0625$ mm) or larger (e.g. $R_d = 1.25$ mm), the strain gradient effects are still significant. For the die radius 1.25 mm, its strain gradient is 0.57/mm, which is rather less than that of the die radius 0.0625 mm (strain gradient 1.78/mm), but the non-dimensional bending moment from the strain gradient theory and the material intrinsic length Eq. (9) is larger than that from classical plasticity theory for 0.06. Moreover, if the sheet thickness is only 0.1 mm, the non-dimensional bending moment increases 0.08 than that of classical plasticity theory for same die radius 1.25 mm. Although the sheet thickness increases almost 10 times (sheet thickness from 0.1 mm up to 1.0 mm), the

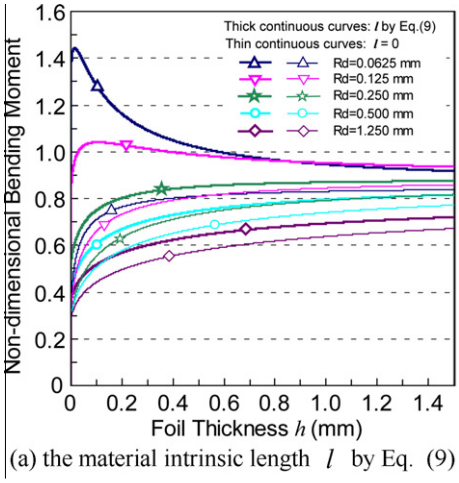

(a) the material intrinsic length l by Eq. (9)

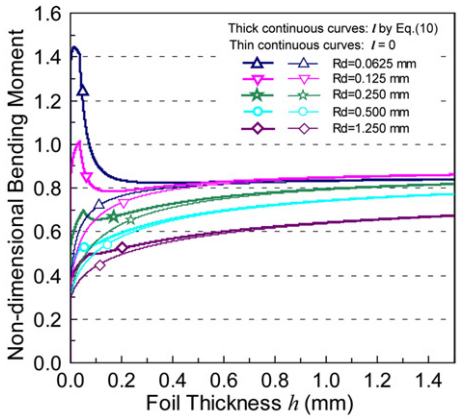

(b) the material intrinsic length l by Eq. (10)

Fig. 11. The non-dimensional bending moment versus the foil thickness.

non-dimensional bending moment decreases only 25% (from 0.08 down to 0.06). In other words, the strain gradient effects are still significant for macro scale sheet bending in Fig. 10a. For the other die radius, the non-dimensional bending moment is still obviously influenced by the strain gradient for the macro scale thickness sheet according to the material intrinsic length Eq. (9).

Fig. 11b shows that there is a inflection point, which is because when the foil thickness is less than the average grain size (i.e. $n_G < 1$), the material intrinsic length is equal to the value of the case of single crystal along the foil thickness direction (i.e. $n_G = 1$). For this case ($n_G < 1$), although the material intrinsic length is constant and the strain gradient (Eq. (23)) become smaller and smaller with the foil thickness increasing, the non-dimensional bending moment will increase because of the surface strain (Eq. (19)) increasing. When the foil thickness exceeds the average grain size ($n_G > 1$), the non-dimensional bending moment will decrease quickly due to the strain gradient effects going down severely together with the material intrinsic length decreasing (Eq. (10)). But for the case of the larger die radius (e.g. $R_d = 1.25$ mm), because of the smaller surface strain (Eq. (19)), the smaller strain gradient, and the more grain numbers across the foil thickness, there exits no obvious inflection point for the non-dimensional bending moment. Fig. 11b shows that when the foil thicknesses are larger than 0.5 mm, the strain gradient effects to the non-dimensional bending moment is rather small. It is worth emphasizing that, for different die radius bending processes, the non-dimensional bending moment predicted from the present strain gradient model can be gradually close to the value predicted from classical plasticity with foil thickness increasing.

Fig. 12 shows the comparison of the non-dimensional bending moment calculated by different analytical models with the experimental data. The non-dimensional bending moment predicted by the classical plastic theory (marked "Classical Plasticity") hardly changes with the foil thickness, and the size effects of the non-dimensional bending moment cannot be predicted at all. The non-dimensional bending moment predicted by strain gradient model (marked "Strain Gradient"), in which the material intrinsic length Eqs. (9) and (10) are used respectively, can show the size effects of the non-dimensional bending moment and the trend is consistent with the experimental data. But the results related with the material intrinsic length Eq. (9) (marked "l by Eq. (9)") are larger than the experimental data especially for the macro scale foils (e.g. thickness 0.2 mm and 0.5 mm), and the result for the foil thickness 0.025 mm is much closer to the experimental data, in which the material intrinsic length is equal to the value by Eq. (10). The predictions of non-dimensional bending moment related with the material intrinsic length Eq. (10) (marked "l by Eq. (10)") agree well with the experimental data. For the foil thickness 0.05 mm and 0.1 mm, the experimental data is underestimated. However, when the foil thickness exceeds 0.2 mm the predictions of non-dimensional bending moment from the present strain gradient model are consistent with that from classical plasticity theory, which is credible to analyze the macro forming. The prediction of non-dimensional bending moment based on the present strain gradient model is much better and reasonable than the results in Ref. (Diehl et al., 2010), in which the experimental data is seriously underestimated for the foil thickness less than 0.05 mm.

All the above-mentioned results show that the material intrinsic length expression Eq. (10) is reasonable for strain gradient hardening model. It is used to predict the springback angle of pure aluminum microbending as following and is proved reasonably too.

4.2. Springback angle prediction

Eqs. (49) and (45) provide the analytical prediction of the springback angle, from which the main influencing factors can be identified. These factors include material elastic properties (especially Young's modulus E), geometrical parameters of the foils and the die set-up (such as foil thickness h, die radius R_d, bending clearance C, etc.), process parameters (such as bending angle θ_b), and the plastic bending moment M_P, which in turn depends on the material intrinsic length l, the parameter K and hardening exponent n etc. In this case, the elastic properties of the material,

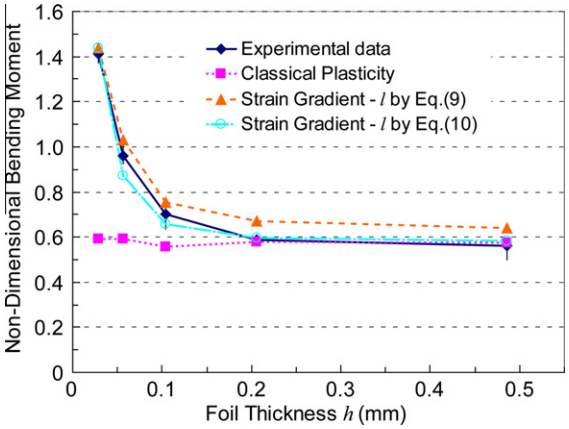

Fig. 12. Comparison of the non-dimensional bending moment with the experimental data.

and the foil thickness, die radius and bending clearance are changed proportionally, so their influence can be neglected, then M_P is the main factor leading to the change of springback angle. The springback angles after microbending are calculated with the analytical model and are compared with the experimental data, as shown in Figs. 13, 14.

Fig. 13a, b, and c show the curves of the springback angle predictions and the experimental data versus the foil thickness for the bending angle 30°, 45°, 65°, respectively. These figures illustrate that the springback angle predicted by the analytical equations based on the classical plasticity theory (marked "Classical Plasticity") are very close to one another. These results hardly change with the foil thickness, in which the curve fluctuation is caused by different values of parameters K, ε_0, n in hardening model for each foil, and the size effects of springback angle cannot be predicted. The smaller the foil thickness is, the larger the difference between the prediction from classical plasticity and the experimental data is. If the proposed constitutive relations with plastic strain gradient hardening are adopted in the analytical model, the results (marked "Strain Gradient") do capture the size effects that the springback angle increases with foil thickness decreasing. Furthermore, the results are close to the experimental data especially for thinner foils. As the foil thickness increases, plastic strain gradient hardening effect gets weaker and weaker, and for the foils thicker than 0.2 mm, the result do not change obviously whether the plastic strain gradient hardening is considered or not.

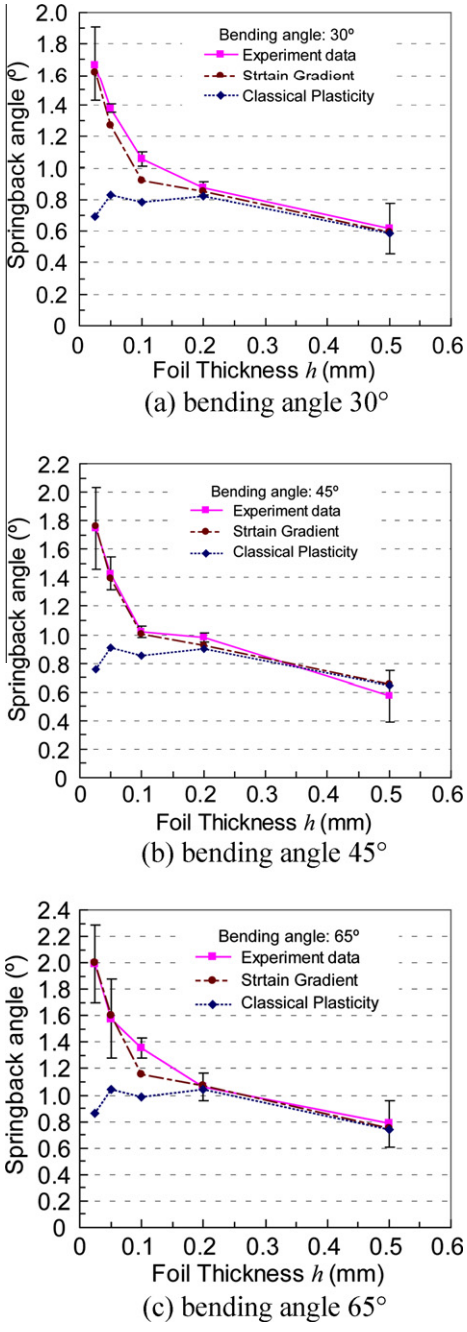

Fig. 13. Springback angle of analysis equations and experimental data versus foil thickness.

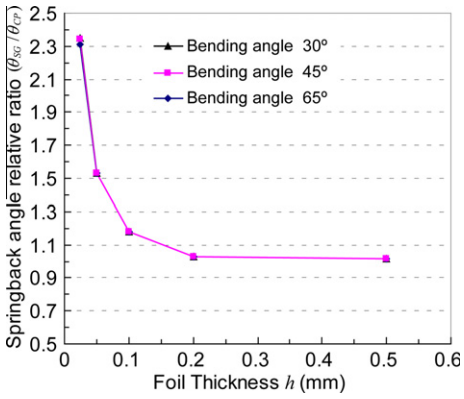

Fig. 14. Contribution of the plastic strain gradient to the microbending springback angle.

Fig. 14 shows the relationship between the relative ratio of springback angle and the foil thickness for bending angle 30°, 45°, 65°, respectively. The vertical axis is the ratio between the springback angle (θ_{SG}) calculated with the proposed constitutive relation with plastic strain gradient hardening and that (θ_{CP}) calculated with the classical plasticity theory ($l = 0$, no considering strain gradient). It shows that the plastic strain gradient hardening effect increases with the foil thickness decreasing, especially when the foil thickness is smaller than 0.2 mm. For the 0.025 mm thickness foil, the ratio of analytical results is greater than 2.0, that is to say, the springback angle is more than doubled because of plastic strain gradient hardening. However, when the foil thickness increases to the macro scale, e.g. 0.5 mm, since the plastic strain gradient hardening effect becomes much weaker, the ratio is close to 1.0, and the results calculated with the classical plasticity theory are acceptable. Fig. 14 also shows that the ratio of springback angle from the strain gradient theory and that from classical plasticity theory is independent on the bending angle. In summary, the contribution of plastic strain gradient to the springback angle increases with the foil thickness decreasing and is independent on the bending angle.

5. Conclusions

Using a scaled method that the experimental set-up dimensions and the foils thickness are changed proportionally, the microbending experiments are carried out for pure aluminum with different thickness from 0.025 mm to 0.5 mm, in which the springback angles are measured by an edge detection algorithm. The experimental data show that the springback angles increase with foil thickness decreasing, especially for foils thinner than 0.1 mm, which indicates obvious presence of size effects.

In order to analyze the size effects, a simplified constitutive model is proposed, which takes into account the plastic strain gradient hardening, and is applied to predict the non-dimensional

bending moment and the springback angle after microbending. The prediction results agree well with experimental data, while those results predicted by the classical plasticity model cannot capture such size effects. It is confirmed that the plastic strain gradient hardening must be taken into account in microbending processes, and it can be omitted for macrobending processes. In microbending process analysis of metal foils, the strain gradient can be simply calculated by the modulus of the gradient of conventional effective plastic strain instead of strain gradient tensor operating.

According to the proposed interaction model between geometrically necessary dislocations and grain boundary, the authors argue that the grain boundary can eliminate the affecting range of geometrically necessary dislocations and reduce the strain gradient hardening. In order to express this effect, the average grain numbers across the foil thickness are considered into the modified material intrinsic length equation. It is more reasonable to predict the non-dimensional bending moment and the springback angle by using the modified material intrinsic length equation.

Acknowledgements

The authors gratefully acknowledge the support from the National Natural Science Foundation of China (Grant No. 50835002, No. 50975174 and No. 50821003) and the German Federal Ministry of Education and Research BMBF (Project No. CHN 08–041). The authors also acknowledge insightful discussions with Prof. Ruan Xueyu of Shanghai Jiao Tong University and the member of the CIRP, Prof. Manfred Geiger of University of Erlangen-Nuremberg on the research.

References

Abu Al-Rub, R.K., Voyiadjis, G.Z., 2005. A direct finite element implementation of the gradient-dependent theory. Int. J. Numer. Meth. Eng. 63, 603–629.
Begley, M.R., Hutchinson, J.W., 1998. The mechanics of size-dependent indentation. J. Mech. Phys. Solids 46, 2049–2068.
Diehl, A., Engel, U., Geiger, M., 2008. Mechanical properties and bending behaviour of metal foils. J. Eng. Manuf. 222, 83–91.
Diehl, A., Engel, U., Merklein, M., Geiger, M., 2010. Size effects in bending processes applied to metal foils. Prod. Eng. 4, 47–56.
Evans, A.G., Hutchinson, J.W., 2009. A critical assessment of theories of strain gradient plasticity. Acta Mater. 57, 1675–1688.
Fleck, N.A., Hutchinson, J.W., 1997. Strain gradient plasticity. Adv. Appl. Mech. 33, 295–361.
Fleck, N.A., Hutchinson, J.W., 2001. A reformulation of strain gradient plasticity. J. Mech. Phys. Solids 49, 2245–2271.
Fleck, N.A., Muller, G.M., Ashby, M.F., Hutchinson, J.W., 1994. Strain gradient plasticity: theory and experiment. Acta Metall. Mater. 42, 475–487.
Gao, H., Huang, Y., Nix, W.D., Hutchinson, J.W., 1999. Mechanism-based strain gradient plasticity - I. Theory. J. Mech. Phys. Solids 47, 1239–1263.
Gau, J.T., Principe, C., Yu, M., 2007. Springback behavior of brass in micro sheet forming. J. Mater. Process. Technol. 191, 7–10.
Geiger, M., Kleiner, M., Eckstein, R., Tiesler, N., Engel, U., 2001. Microforming. Ann. CIRP. 50, 445–462.
Haque, M.A., Saif, M.T.A., 2003. Strain gradient effect in nanoscale thin films. Acta Mater. 51, 3053–3061.
Huang, Y., Gao, H., Nix, W.D., Hutchinson, J.W., 2000. Mechanism-based strain gradient plasticity - II. Analysis. J. Mech. Phys. Solids 48, 99–128.
Lee, R.S., Chen, H.C., Gau, J.T., 2008. Effect of thickness to grain size ratio on drawability for micro deep drawing of AISI 304 stainless steel ICTP, pp. 183–188.
Li, J.C.M., Chou, Y.T., 1970. The role of dislocation in the flow stress grain size relationships. Metall. Trans. B. 1, 1145–1159.
McElhaney, K.W., Vlassak, J.J., Nix, W.D., 1998. Determination of indenter tip geometry and indentation contact area for depth-sensing indentation experiments. J. Mater. Res. 13, 1300–1306.
Nix, W.D., Gao, H.J., 1998. Indentation size effects in crystalline materials: A law for strain gradient plasticity. J. Mech. Phys. Solids 46, 411–425.
Parasiz, S.A., VanBenthysen, R., Kinsey, B.L., 2010. Deformation size effects due to specimen and grain size in microbending. J. Manuf. Sci. Eng. 132. 011018. 1-8.
Stölken, J.S., Evans, A.G., 1998. A microbend test method for measuring the plasticity length scale. Acta Mater. 46, 5109–5115.
Suzuki, K., Matsuki, Y., Masaki, K., Sato, M., Kuroda, M., 2009. Tensile and microbend tests of pure aluminum foils with different thicknesses. Mat. Sci. Eng. A. 513-514, 77–82.
Taylor, G.I., 1938. Plastic strain in metals. J. Inst. Metals 62, 307–324.
Voyiadjis, G.Z., Abu Al-Rub, R.K., 2005. Gradient plasticity theory with a variable length scale parameter. Int. J. Solids. Struct. 42, 3998–4029.
Wang, W., Huang, Y., Hsia, K.J., Hu, K.X., Chandra, A., 2003. A study of microbend test by strain gradient plasticity. Int. J. Plast. 19, 365–382.
Xue, Z., Huang, Y., Li, M., 2002. Particle size effect in metallic materials: a study by the theory of mechanism-based strain gradient plasticity. Acta Mater. 50, 149–160.
Yuan, H., Chen, J., 2001. Identification of the intrinsic material length in gradient plasticity theory from micro-indentation tests. Int. J. Solids. Struct. 38, 8171–8187.
Zbib, H.M., Aifantis, E.C., 2003. Size effects and length scales in gradient plasticity and dislocation dynamics. Scripta. Mater. 48, 155–160.
Zhu, H.X., Karihaloo, B.L., 2008. Size-dependent bending of thin metallic films. Int. J. Plast. 24, 991–1007.